Received: 5 December 2019 | Revised: 25 February 2020 | Accepted: 6 March 2020

DOI: 10.1096/fj.201903049R

RESEARCH ARTICLE

THE FASEB JOURNAL

Stimulation of water and calcium dynamics in astrocytes with pulsed infrared light

Ana I. Borrachero-Conejo[1] | Wilson R. Adams[2,3] | Emanuela Saracino[4] | Maria Grazia Mola[5] | Manqing Wang[3,6] | Tamara Posati[4] | Francesco Formaggio[7] | Manuela De Bellis[5] | Antonio Frigeri[8,9] | Marco Caprini[1,7] | Mark R. Hutchinson[10] | Michele Muccini[1] | Roberto Zamboni[4] | Grazia Paola Nicchia[4,5,9] | Anita Mahadevan-Jansen[2,3,11] | Valentina Benfenati[4]

[1]Istituto per lo Studio dei Materiali Nanostrutturati, Consiglio Nazionale delle Ricerche, Bologna, Italy

[2]Department Biomedical Engineering, Vanderbilt University, Nashville, TN, USA

[3]Vanderbilt Biophotonics Center, Vanderbilt University, Nashville, TN, USA

[4]Istituto per la Sintesi Organica e la Fotoreattività, Consiglio Nazionale delle Ricerche, Bologna, Italy

[5]Department of Bioscience, Biotechnology and Biopharmaceutics and Centre of Excellence in Comparative Genomics, University of Bari Aldo Moro, Bari, Italy

[6]Bioengineering College, Chongqing University, Chongqing, China

[7]Dipartimento di Farmacia e Biotecnologie, University of Bologna, Bologna, Italy

[8]Department of Basic Medical Sciences, Neuroscience and Sense Organs, School of Medicine, University of Bari Aldo Moro, Bari, Italy

[9]Department of Neuroscience, Albert Einstein College of Medicine, Yeshiva University, New York, NY, USA

[10]Australian Research Council Centre of Excellence for Nanoscale BioPhotonics, Adelaide Medical School, University of Adelaide, Adelaide, SA, Australia

[11]Department of Neurological Surgery, Vanderbilt University Medical Center, Nashville, TN, USA

Correspondence
Anita Mahadevan-Jansen, Department Biomedical Engineering, Vanderbilt University, 5824 Stevenson Center, Nashville, TN 37232, USA.
Email: anita.mahadevan-jansen@vanderbilt.edu

Valentina Benfenati, Consiglio Nazionale delle Ricerche, Istituto per la Sintesi Organica e la Fotoreattività, via Gobetti, 101, Bologna 40129, Italy.
Email: valentina.benfenati@isof.cnr.it

Abstract

Astrocytes are non-neuronal cells that govern the homeostatic regulation of the brain through ions and water transport, and Ca^{2+}-mediated signaling. As they are tightly integrated into neural networks, label-free tools that can modulate cell function are needed to evaluate the role of astrocytes in brain physiology and dysfunction. Using live-cell fluorescence imaging, pharmacology, electrophysiology, and genetic manipulation, we show that pulsed infrared light can modulate astrocyte function through changes in intracellular Ca^{2+} and water dynamics, providing unique mechanistic insight into the effect of pulsed infrared laser light on astroglial cells. Water transport is activated and, IP_3R, TRPA1, TRPV4, and Aquaporin-4 are all involved

Abbreviations: 2-APB, 2-Aminoethoxydiphenylborane, IP_3R antagonist; AQP4, aquaporin-4; Ca^{2+}, calcium ions; CBX, carbenoxolone, gap junction antagonist; HC, HC030031, TRPA1-specific antagonist; HTlc, hydrotalcite; INS, infrared neural stimulation; IP_3R, inositol-3-phosphate receptor; IR, infrared; KO, knock out; NIR, near infrared, 750-1000 nm light; PDL, Poly-D-lysine; RN, RN-1734, TRPV4-specific antagonist; RR, ruthenium red, broadband TRP antagonist; SEM, standard error of the mean; siRNA, small interference ribonucleic acid sequence; TPEN, (N,N,N′,N′-tetrakis(2-pyridinylmethyl)-1,2-ethanediamine, intracellular calcium chelator; TRPA1, transient receptor protein ankyrin type 1; TRPV4, transient receptor protein vanilloid type 4; WT, wild-type.

Ana I. Borrachero-Conejo and Wilson R. Adams are equally contributed to this work.

Funding information
EU, Grant/Award Number: GA 316832; ASEE; AFOSR, Grant/Award Number: FA9550 16-1-0502, FA9550-17-1-0502, FA9550-15-1-0328, FA9550-14-1-0303, FA 9550-17-1-0374 and FA9550-18-1-0255; NIH, Grant/Award Number: CA68485, DK20593, DK58404, DK59637 and EY08126

in shaping the dynamics of infrared pulse-evoked intracellular calcium signal. These results demonstrate that astrocyte function can be modulated with infrared light. We expect that targeted control over calcium dynamics and water transport will help to study the crucial role of astrocytes in edema, ischemia, glioma progression, stroke, and epilepsy.

KEYWORDS
AQP4, astrocytes, infrared stimulation, TRPV4, water dynamics

1 | INTRODUCTION

The ability of the brain to receive and process information is critically dependent on regulation operated by nonneuronal cells called astrocytes.[1,2] Astrocytes sense variation of extracellular milieu composition that occur in the extracellular environment during and following neuronal activity. These variations trigger selective activation of transmembrane receptors and channels leading to ion, water, and Ca^{2+} fluxes among others across the cell membrane. The latter membrane dynamics can orchestrate processes such as energetic delivery, vascular activity, and even immune responses depending on the stimulus.[1,3,4]

Various receptors and channels have been implicated in the mechanisms of astrocytes. Among others, plasma membrane cation channels belonging to the transient receptor potential (TRP) superfamily have been shown to play a critical role in regulating homeostatic intracellular calcium ($[Ca^{2+}]_i$) signaling in astroglia.[5-11] Water transport and distribution is facilitated by the water channel aquaporin-4 (AQP4).[11-13] Together, TRP Vanilloid 4 (TRPV4) channels in conjunction with AQP4 are critical in controlling ion and water dynamics, thus, driving regulatory volume mechanisms as shown in primary astrocytes[11,14] and the retina in situ.[13,15] Dysfunction in this TRPV4-AQP4 cooperation causes brain swelling, most notably in ischemia, epilepsy, and brain tumors, proving the importance of astrocytes in the homeostatic mechanism for normal brain physiology.[6,12,16]

The narrow set of tools currently available to modulate ion fluxes, water dynamics, and numerous receptors and channels expressed in astrocytes have limited our ability to effectively study their importance in healthy and pathological brain function. Methods to study astrocytic processes have been for a long time confined to conventional pharmacology, genetic manipulation, fluorescence imaging of molecular sensors, and electrophysiology.[3,5,11,14,17-19] More recently, we demonstrated that it is possible to evoke chloride ion conductances,[20] astrocytic Ca2+ responses mediated by TRPV4 and cell swelling by optical or electrical stimulation operated by organic devices.[21] Optical tools can provide precise, fast, label-free control of ions, and water dynamics to study the cellular and molecular mechanisms of astrocytes function and to potentially treat dysfunction. However, despite recent advances in optogenetics approaches and optoelectronics device to study neurons,[22,23] there is a continued need for reliable methods for label-free control of ion flux and water dynamics in astrocytes.[19,21,22,24]

Infrared stimulation is a label-free approach that can modulate neural activity in cells and tissues by transient delivery of pulsed infrared laser light.[25-29] Mechanistically, infrared stimulation has been shown to rely on a transient spatial and temporal thermal gradient for neuronal depolarization and action potential initiation in the peripheral and central nervous system.[30-32] Studies have also demonstrated the ability of infrared stimulation to modulate processes in different cells. However, the biophysical mechanisms, by which this method modulates cells and tissues is not fully understood.[30,32] Nonetheless, the direct effect of pulsed infrared light on nonneuronal cells such as astrocytes has not been previously reported.

The goal of this paper then is to study the effect of pulsed infrared light on astrocytes and to understand the mechanisms, by which astrocytes may be modulated. Results show that infrared stimulation can drive Ca^{2+} dynamics, trigger water transport, and cell volume changes in rodent astrocytes. Based on our observations of the activation of TRP channels, inositol-3-phosphate receptor (IP_3R) and AQP4, we propose the molecular mechanisms, by which astrocytes are modulated with infrared light. These findings suggest that infrared stimulation offers a transformative approach to study astrocytic homeostatic regulation and to study glial involvement in normal and diseased brain physiology as well as in the clinical care of brain disease.

2 | MATERIALS AND METHODS

2.1 | Rat cortical astrocyte culture preparation, maintenance, and plating

Primary astroglial cultures were prepared at the University of Bologna (UNIBO) and at the University of Bari (UNIBA), in concordance with the Italian and European law of protection of laboratory animals, with the approval of the local bioethical committee and under the supervision

of the veterinary commission for animal care and comfort of UNIBO and UNIBA, with approved protocol from Italian Ministry of Health (n° 360/2017-PR for UNIBO and 710/2017-PR for UNIBA). Astrocytes primary culture were prepared as described previously.[3,5,11] Neonatal cerebral occipital cortices from newborns, at postnatal day 1-2, of Rattus, Norvegicus, Wistar devoided of meninges were gently triturated, filtered with a 70-lm cell strainer (Falcon, BD Bioscience, Bedford, MA), and placed in cell culture flasks containing Dulbecco's Modified Eagle-glutamax medium with 15% of fetal bovine serum (FBS) and penicillin/streptomycin (100 U/mL and 100 lg/mL, respectively) as described previously.[11] AQP4 KO ($^{-/-}$) pups with a CD21 genetic background and aged-matched controls were used for preparation of primary cortical astrocytes as described previously.[14]

Cells were maintained in incubation at 37ºC and 5% of CO2 and proper humidity levels for three weeks. During this period, we replaced cell medium every three days and flasks were gently shaken when necessary to remove undesired cells. After three and four weeks after isolation cells were detached using trypsin/EDTA 0.025% of solution for 5 minutes at 37ºC and 5% of CO_2.

Primary confluent astrocytes were re-suspended by using Trypsin-EDTA and re-plated on Glass coverslips coated with Poly-D-lysine (PDL) or with hydrotalcite (HTlc) films, prepared as described previously.[33] Experiments were performed 48-72h after re-plating. Astrocytes were plated at a high density for calcium imaging and calcium quenching experiments (2.5×10^4 cells/19 mm coverslips). For single-cell patch-clamp experiments, cells were seeded at a low density (10^4 cells/33 mm Petri dish).

2.2 | Pulsed infrared laser stimulation

To explore the effect of pulsed infrared light on astrocytes, an inverted epifluorescence microscope was fitted with a multimode fiber attached to a micromanipulator (Sutter Inc), ensuring tight control of optical fiber positioning at close proximity (230-250 μm) to primary astrocytes plated on a glass coverslip (Figure 1A,B). Laser light at 1875 nm from a pulsed diode laser (Capella, Lockheed Martin Aculight, Bothell, WA) was coupled to the fiber. The pulse duration was set to 8 ms, which was calculated to be ~3 J/cm2 at the sample plane and was delivered 30 seconds after the beginning of the experiment. The infrared laser output was estimated to be located ~240 μm from the center of the optical fiber face at a 45° angle to the cell-coverslip plane (Figure 1B). For pharmacological characterization of astrocyte responses, an exposure to elicit a target activation probability of 0.8 was used as a baseline for comparison across all experiments.

2.3 | Transfection with siRNA

SiRNA transfection was performed using Lipofectamine RNAiMAX and Opti-MEM according to manufacturer instructions (Invitrogen) and to protocols previously described.[11] Briefly, Stealth RNAi siRNA select RNAi (ID RSS330373, designated "number 9") that in turn target nucleotides 1201-1225, of rat TRPV4 (GenBank accession no. NM_023970.1) were purchased from Invitrogen. Transfection was performed on two-three weeks-old primary rat astrocytes using Lipofectamine RNAiMAX and Opti-MEM I reduced serum medium according to the manufacturer's instructions (Invitrogen). The day before transfection, astrocytes were cultured using DMEM with 10% of FBS without antibiotics. The final concentrations were 50 nM for the selected RNAi or scrambled control and 10 μL for Lipofectamine RNAiMAX in a 60-mm culture vessel. After 24 hours the medium was replaced with complete 10% of FBS DMEM containing penicillin/streptomycin (100 U/mL and 100 μg/mL, respectively) medium. Transfection efficiency was verified using a BLOCK-iT Alexa Fluor Red Fluorescent Oligo that is not homologous to any known genes. Five days after transfection, we performed calcium imaging experiments as described above.

2.4 | Western blot analyses

After 5 days from transfection, Western blot analyses was performed on cells transfected with scrambled siRNA and TRPV4 siRNA, as described previously.[11] Briefly, samples containing 25 μg total protein were separated on SDS-polyacrylamide gels and electrotransferred on to nitrocellulose membranes (Bio-Rad Laboratories), blocked in 5% of BSA in PBS containing 0.05% of Tween-20 and probed overnight at 4°C with primary antibodies against TRPV4 (1:500, Alomone Laboratories, Jerusalem, Israel), or Actin (1:1000, Sigma-Aldrich). After washing with phosphate-buffered saline plus Tween 0.05% v/v (PBST) membranes were incubated with horseradish peroxidase-conjugated IgG secondary antibodies (Sigma) and developed with ECL-Plus (Bio-Rad). Blot imaging and densitometric analyses were performed with Chemidoc software (Bio-Rad).

2.5 | Calcium imaging

Changes in intracellular Ca^{2+} concentration ($[Ca^{2+}]i$) were monitored by calcium imaging using the single-wavelength Ca^{2+} indicator Fluo-4-AM (Life Technologies). Experiments were performed 48 hours after cell plating. Astrocytes plated in glass + PDL and HTlc samples were incubated at room temperature for 45 minutes to 1 hour with Fluo-4-AM (1

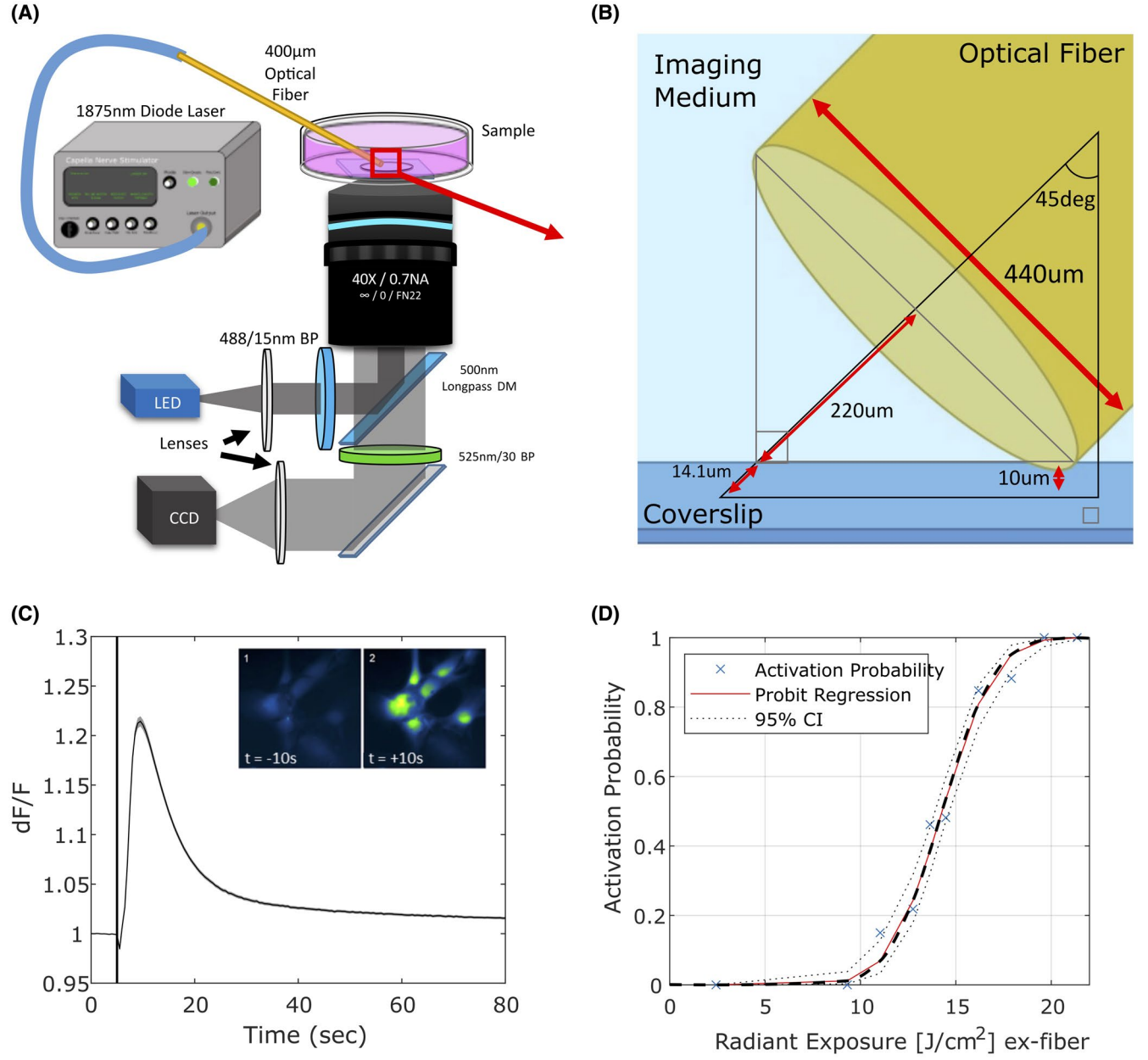

FIGURE 1 Pulsed infrared light can stimulate calcium imaging in cultured astrocytes. A, Schematic representation of the experimental set-up for stimulation of astrocyte (λ=1875 nm). B, To-scale illustration of fiber placement in proximity of cells during the experiments. C, Representative trace depicting the normalized variation in cell fluorescence over time (dF/F) that reflects variation in $[Ca^{2+}]_i$. Red dashed line marks the timepoint at which laser pulse was delivered. Inset. Fluorescent images of Fluo-4-AM loaded astrocytes captured before the stimulation (1, t = 0s) and at the peak of fluorescence after stimulation (2, t = 12 s), scale bar is 40 µM. D, Activation probability (P) as a function of radiant exposure delivered to rat primary astrocytes

uM) dissolved in control saline solution. Measurements of $[Ca^{2+}]_i$ were performed by using an epifluorescence microscope (Nikon Eclipse Ti-S) equipped with long-distance dry objective (40x, 0.4NA) and standard filters for GFP fluorescence. The excitation wavelength was 470 nm, filtered from a broadband LED light source. Light pulse durations were set to 200 ms, while camera exposure times were set to 100 ms with a sampling rate of 2 Hz. Data acquisition was controlled by MetaFluor software (Molecular Devices, Sunnyvale, CA, USA) or NIS Elements (Nikon Imaging Systems).

2.6 | Electrophysiology

Current recordings were obtained with the whole-cell configuration of the patch-clamp technique as described previously.[5] Patch pipettes were prepared from thin-walled borosilicate glass capillaries to obtain a tip resistance of 2-4 MΩ when filled with the standard internal solution. Membrane currents were amplified, filtered at 2 kHz, and acquired at a sample rate of 5 kHz by Axopatch 200B amplifier in voltage-clamp mode. Responses were amplified, low-pass filtered at 1 kHz,

digitized at 20 kHz, stored, and analyzed with pCLAMP 10. Liquid junction potential (7 mV) was calculated and corrected off-line; voltages indicated are those relative to the real transmembrane potentials. Experiments were carried out at room temperature (22-24°C). When necessary, current values were plotted as current densities calculated by dividing the current values measured at each membrane potential by the cell capacitance obtained by the correction of the capacitive transient of the recorded cells by means of the digital circuit of the patch-clamp amplifier. To investigate whether astrocytic TRPV4 conductance was altered by INS, we performed whole-cell patch-clamp experiments, according to protocols described previously[5,6] by holding the membrane potential (Vh) at 7 mV and stimulating the cells with a 400-ms-long step potential to −87 mV, followed by a voltage ramp from −87 to 73 mV for 600 ms Potassium (K^+) in the intra- and extra-cellular saline were replaced by cesium (Cs^+) to isolate TRPV4 conductance from voltage-gated K^+ currents expressed by astrocytes in vitro and in situ. Moreover, intracellular Cl^- was partially replaced by gluconate to change reversal potential of Cl^- and to distinguish chloride currents from cationic ones. The outward rectification profile, known to be dependent by $[Ca^{2+}]_o$, caused by Ca^{2+} blockage at membrane potentials negative to the reversal potential (E_{rev}) was prevented by using 2 mM $[Ca^{2+}]_o$. infrared neural stimulation (INS) pulse was delivered when current profiles reached the steady-state.

2.7 | Calcein self-quenching image acquisition

Changes in cell volume were assessed using calcein fluorescence quenching as described previously.[14,34] Experiments were performed 48-72h after cell re-plating. Astrocytes were loaded with Calcein-AM (10 μM) (Life Technologies, USA) dissolved in standard bath solution and they were incubated for 30 minutes at room temperature. Image acquisition was controlled by the NIS Elements (Nikon Imaging Systems) on a Nikon TI-Eclipse inverted epifluorescence microscope (Nikon Instruments). The excitation wavelength used was 470 nm filtered from a broadband source and fluorescence from calcein was filtered through a standard GFP filter cube (Nikon Instruments). Cells were imaged through a 20X/0.7NA air objective (Nikon) with a sCMOS camera (Hamamatsu Orca Flash 4.0). Camera exposure time of 10 ms and a sampling rate of 5 Hz was employed.

Image processing and analysis were done in FIJI[35] and Matlab (Natick, MA, USA). Time course fluorescence data were analyzed with Prism (Graph Pad, San Diego, CA, USA) software. For each experimental curve, the time constant of cell swelling or shrinkage phase was obtained by fitting the data with an exponential function and a time constant calculated.[34] Further details surrounding data analysis can be found in Supporting Information.

2.8 | Solutions and chemicals

Calcium imaging and calcein self-quenching analyses the control saline bath solution, named as control (CTRL) was composed of (mM): 140 NaCl, 4 KCl, 2 $MgCl_2$, 2 $CaCl_2$, 10 HEPES, 5 glucose, pH 7.4 with NaOH and osmolarity adjusted to ~318 mOsm with mannitol. Ca^{2+}-free extracellular solution (0 $[Ca^{2+}]_{out}$) contained (mM) 140 NaCl, 4 KCl, 4$MgCl_2$, 10 HEPES, 0.5 EGTA, pH 7.4 with NaOH and osmolarity adjusted to ~318 mOsm with mannitol. For electrophysiological experiments, the standard bath saline was (mM) 140 NaCl, 4 KCl, 2 MgCl2, 2 CaCl2, 10 Hepes, 5 glucose, pH 7.4 with NaOH and osmolarity adjusted to 315 mOsm with mannitol. In order to eliminate potassium currents, K^+ was omitted by extracellular solution and pipette solutions was replaced with cesium (Cs). The intracellular (pipette) solution was composed of (mM): 100 Cs gluconate, 26 CsCl2, 2 MgCl2, 1 EGTA, 10 TES, pH 7.2 with CsOH and osmolarity 300 mOsm with mannitol.

Salts and chemicals used to prepare physiological solutions were the highest purity grade and obtained from Sigma (Milan, Italy).

2.9 | Data analysis, representation, and statistics

All data are expressed as mean of several cells (n) ± SEM. Statistical comparison of metrics is performed with a 2-sided student's t test unless otherwise noted. A P-value $< .05$ was considered statistically significant. All analyses were performed in Matlab.

2.9.1 | Calcium imaging

On the basis of previous study,[5,11] considering the consistency of the results obtained in previous works using the same culture preparation, we determinate that a minimum number of four recordings (n value) from three different animals with two replicates (coverslips) can be considered significant sample size to determine the response of astrocytes to INS and for the pharmacological manipulation. Accordingly, each cell culture preparation was prepared from one different newborns animal and each calcium imaging recording was considered as n (N). For each experimental condition, a set of at least two different coverslips from each cell culture preparation were tested. For patch-clamp experiments, a minimum of 10 cells recorded with the same ionic condition were

considered significant sample size for testing the response to INS, and 4 when pharmacology was used TRP pharmacology.[5,11,36] Somatic cellular fluorescence time series were manually extracted in both Metafluor (Molecular Devices, Sunnyvale, CA, USA) and with a custom-written FIJI script to accelerate data extraction.[35] Extracted data were imported into analysis in MATLAB (Mathworks, Natick, MA, USA), where raw fluorescence traces are aligned relative to INS pulse delivery, normalized, and processed to extract different calcium response metrics. Alignment of traces relative to INS pulse delivery were performed by locating the peak second derivative for fluorescence intensity as a function of time for each imaging experiment's average time series. Defocusing due to the transient heating of the INS pulse delivery yields a sharp transient decrease in observed intensity for each image, which resulted in a relatively high peak in the fluorescence time series second derivative. Time series data for each cell was subsequently truncated to 5 seconds prior to INS exposure for analysis purposes. Each cell's raw fluorescence intensity was normalized with respect to the mean raw intensity of the 10 frames prior to IR exposure, which are reported and analyzed as fractions (dF/F).

Quantitative metrics extracted from each cell's time series trace included maximum change in relative fluorescence, elapsed time to peak fluorescence intensity, the full-width half-maximum of each cells response, and the numerically integrated area of each cell's response. A cell was deemed "activated" if a 5% increase in normalized calcium fluorescence within 20 seconds of IR exposure. The fraction of activated cells relative to the total number of cells observed is reported as "activation fraction" or "fraction of responding cells". Statistical comparison of metrics is performed with a 2-sided student's *t* test unless otherwise noted. Error bars reported are standard error of the mean (SEM) response between cells unless otherwise denoted. Plotting was performed in MATLAB with the "superbar" package and native plotting functions. FIJI scripts for data compression/extraction as well as MATLAB processing scripts are available upon request.

2.9.2 | Analysis of calcein experiments

For analysis of calcein experiments, cells were selected, and time series were extracted through a custom FIJI script. Time series for each cell were imported into MATLAB for processing and analysis. Low-frequency fluorescence background subtraction from each time series was achieved by fitting a 6th-order polynomial function the time series points outside of our region of interest. Our determined area of interest was 5 frames prior to INS stimulus and 350 after stimulus. The initial 50 frames of data were excluded to avoid skewed fits due to initial photobleaching artifacts. We found that the 6th-order polynomial best accounted for photobleaching inconsistencies that arise from preparing each field of view for observation (eg, fiber placement). Relative changes in calcein fluorescence due to INS exposure were calculated by dividing the difference of corrected fluorescence intensity 2 seconds[10] prior to and following INS exposure by the pre-stimulated fluorescence intensity (dF/F). Negative changes in fluorescence indicate decreases in fluorescence intensity after INS exposure. Mean time traces are reported for each experimental condition as the central tendencies of observed responses, unless otherwise noted.

2.9.3 | Electrophysiological data

Electrophysiological data are expressed as mean ± standard error mean (SEM) of several cells (n) in the various conditions. The statistical analysis was performed with two-tailed Student's *t* test and a *P*-value .05 was taken as statistically significant. Steady state current density in response to ramp currents was calculated before and after the INS stimulation. Maximal current increase (ΔpA/pF) is reported as the ratio of the maximal current density observed after INS at −87 mV and +73 mV, divided by the current density recorded at the same voltages at the steady state before the stimulus.

3 | RESULTS AND DISCUSSION

3.1 | Infrared pulsed stimulation evokes calcium signaling in primary astrocytes

To evaluate whether pulsed infrared light can modulate astrocytes, cortical primary rat astrocytes were plated on glass coverslips coated with Poly-D-lysine (PDL) and placed under an inverted fluorescence microscope while delivering 8 ms pulsed infrared light (λ = 1875 nm) using an optical fiber placed close to the cell from above as shown in Figure 1 (See Methods). The astrocytes were loaded with the calcium indicator Fluo-4-AM (2 μM) and calcium imaging was used to study the resulting cell dynamics. Changes in fluorescence intensity (dF/F) were directly related to intracellular levels of free Ca^{2+} ($[Ca^{2+}]_i$) in the cell soma. The observed responses were characterized by a rapid increase in $[Ca^{2+}]_i$ that reached its peak intensity ~6.91 ± 1.12 seconds (T_{peak}) and had a duration ($T_{1/2}$, reported as full-width half-maximum times) of 9.39 ± 1.64 seconds, followed by a recovery of fluorescence to near initial baseline levels after 120 seconds (Figure 1C). The time course of dF/F response of an individual cell were consistent across the cells observed with an average maximum fluorescence of 1.28 ± 0.02. The activation probability (P), or the fraction of cells responding to infrared light, was found to be dependent on radiant exposure (J/cm^2) with a 50% activation probability occurring at 14.31 J/cm^2 at the tip of the fiber (Figure 1D), which

translates to approximately 3 J/cm^2 at the cell surface. Radiant exposures targeting an activation fraction of 0.8 was selected for the rest of the experiments described. We have performed experiments to verify astrocytic viability during IR stimulation by assessing extracellular membrane integrity with propidium iodide (PI) uptake. By exposing cells to IR in the presence of PI-containing solution, positively stained cell nuclei would indicate cell death induced by the IR pulse. Unstimulated (Figure S1A) and threshold-stimulated cells (Figure S1B) showed negligible levels of PI fluorescence, within 5 minutes of IR stimulation. On the contrary, exposure to IR at almost higher power (Figure S4C) and to chemogenic permeabilization with a dilute detergent solution, 0.1% Tween-20 (Sigma-Aldrich, St. Louis, MO, USA) (Figure S1D) display strong PI fluorescent signal. Collectively, these results suggest that, within 5 minutes of IR stimulation, acute cellular damage is not a cause for concern at threshold radiant exposures for astrocytic modulation.

Pharmacological methods were used to isolate the basis of intracellular Ca^{2+} rise observed with infrared stimulation. All the results, expressed as mean ± SEM and statistic *P*-values (*P*val), are reported in Supporting Table S1. Application of intracellular Ca^{2+} chelator (N,N,N′,N′-tetrakis(2-pyridinylmethyl)-1,2-ethanediamine, TPEN, 2mM)[37] (Supporting Table S1, Figure 2, and Figure S2) results in a significant reduction in activation probability and peak dF/F followed by alterations in response dynamics. Application of 2-Aminoethoxydiphenylborane (2-APB, 100 μM), an antagonist of Inositol-3-Phosphate (IP_3) receptors results in a near loss of the calcium response and a drastic reduction in activation probability. Substitution of control saline solution (CTRL) with a Ca^{2+}-free solution (0$[Ca^{2+}]_o$, Figure 2A,B) results in a statistically significant decrease in dF/F and $T_{1/2}$ and a decrease in the activation probability as well as < T_{peak} (Table S1, Figure 2, Figure S2) and shows that extracellular Ca^{2+} influx is needed for the amplification and maintenance of infrared-mediated $[Ca^{2+}]_i$ responses as well as the onset of Ca^{2+} response. We found that blocking gap junctions (essential for propagation of $[Ca^{2+}]_i$ through the syncytium[38,39] does not alter the magnitude of $[Ca^{2+}]_i$ responses when compared to control, as observed with bath application of Carbenoxolone (CBX) although the activation probability is significantly reduced. Collectively, our results suggest that $[Ca^{2+}]_i$ responses to pulsed infrared light are initiated by IP_3R-dependent Ca^{2+} release from intracellular stores, sustained by $[Ca^{2+}]_o$ influx, and propagated across astroglia cellular networks through gap junction.[38]

These observations align with the response to infrared stimulation seen in neuroblastoma-glioma and hippocampal neurons in vitro.[40,41] Pharmacology implicates IP_3R as a primary pathway for the release of $[Ca^{2+}]_i$ from intracellular stores and is believed to be critical in numerous astrocytic functions.[1,2] Recent work suggested that Ca^{2+} release via IP_3R activation is crucial for the release of signaling molecules from astrocytes that mediate astrocyte-neuronal communication and influence long term potentiation in situ.[2,42] Thus, our results with an approach that can trigger IP_3R pathways might offer the opportunity for probing communication between neuronal and glial cells.

3.2 | TRPV4 and TRPA1 mediate influx of calcium and whole-cell conductance changes with infrared light

Using selective pharmacology and siRNA methodologies, the molecular basis for $[Ca^{2+}]_o$ influx was evaluated. Thermally sensitive TRPV4 has been shown to be involved in the response of spiral, vestibular, and dorsal root ganglion neurons to pulsed infrared light.[43-45] Considering TRPV4's role in astrocyte physiology,[5-6,13] we postulated that TRPV4 is involved in the Ca^{2+} dynamics of astrocytes during infrared stimulation. Results show that TRP superfamily member channels are broadly involved in Ca^{2+} influx. The magnitude of dF/F and activation probability is significantly reduced following the application of a broad-spectrum TRP channel antagonist, Ruthenium Red (RR, 10 μM) (see Figure 2E,F). Additionally, RR did not alter the dynamics of Ca^{2+} responses, as T_{peak} and $T_{1/2}$ when using RR is comparable to values in control saline (Figure S2C,D). In the presence of selective TRPV4 antagonist RN1734 (RN, 10 μM),[46] dF/F, and activation probability were reduced but not eliminated, and it is not involved in shaping the response dynamics (Figure S2C,D). These findings indicate that TRPV4 is important in the observed response but is not the sole intermediary to the process. With the addition of HC030031 - a TRP Ankyrin-1 (TRPA1)-specific antagonist - the peak dF/F was significantly attenuated, while T_{peak} and $T_{1/2}$ both increased (Figure S2C,D). On the contrary, activation probability was not significantly altered (Figure 2D,F). These results support that TRPA1 also plays a role in the magnitude and dynamics of the Ca^{2+} responses.

Figure 3 shows the results obtained in astrocytes transfected with scrambled siRNA and TRPV4 siRNA. Western blot experiments and densitometric analysis, indicated that the transfection with TRPV4 siRNA causes 73% (±4%) of reduction of the band at 110 kDa, which correspond to the isoform that is expressed in the membrane of astrocytes[5] (Figure S3A).

Reduced expression of TRPV4 alter Ca^{2+} responses with infrared stimulation (Figure 3A). Slight but significant differences were observed in the T_{peak} (Figure S3B), while $T_{1/2}$ was significantly higher in TRPV4 knock down cells (Figure S3C). Both *df*/F and activation probability are significantly lower in these cells (Figure 3B,C). Using a whole-cell patch-clamp rig, electrophysiology was also performed in transfected astrocytes as well as nontransfected cells (Figure 3D,E).

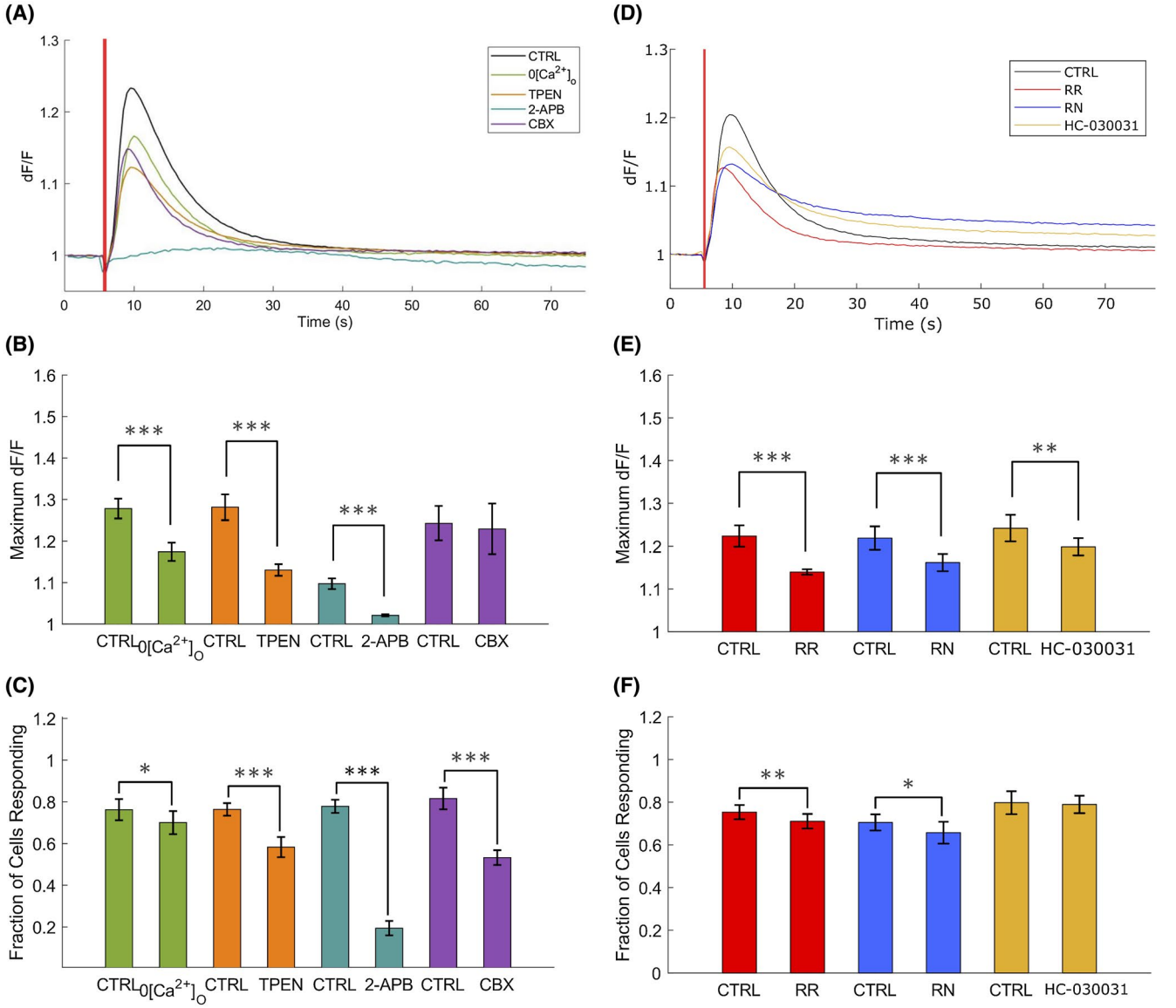

FIGURE 2 Pharmacology of the $[Ca^{2+}]_i$ response of astrocytes to infrared light. A, Representative traces of experiments performed using extracellular standard solution (black, CTRL), extracellular solution not-containing Ca^{2+} ($0[Ca^{2+}]_o$, green trace), and by adding TPEN (2mM, orange trace), 2-APB (100 μM, blue trace) or CBX (50 μM, violet trace) to the CTRL saline. B and C, Histogram plots depicting the averaged maximal dF/F (B) and activation probability (C) calculated for CTRL saline and $0[Ca^{2+}]_o$ solution (green columns), CTRL and CTRL + TPEN (orange columns), CTRL and CTRL + 2-APB (blue columns), CTRL and CTRL + CBX (purple columns). D, Representative traces of experiments performed in CTRL saline (black), and CTRL + Ruthenium Red (RR, 10 μM, red trace), CTRL + RN-1734 (10 μM, dark blue trace), CTRL + HC-030031 (40 μM, yellow trace). E and F, Histogram plots depicting the averaged maximal dF/F (E) and activation probability (F) calculated using CTRL saline and CTRL + RR (10 μM, red columns), CTRL and CTRL + RN-1734 (10 μM, dark blue columns), CTRL and CTRL + HC-030031 (40 μM, yellow columns). Data are reported as mean and SEM. Student's *t* test, $*P < .05$; $**P < .01$; $***P < .001$). Red lines in A and D represent the time point at which the pulsed infrared light was delivered. All experiment in the present figure were performed using primary rat cortical astrocytes

The electrophysiological data further implicate the role of TRPV4, demonstrating that infrared-induced cationic current increases are attenuated upon knocking down the expression of TRPV4. Cationic currents are further abolished by additional blocking the function of TRPA1 (Figure 3E). Using saline solution and stimulation protocols described previously,5,6 we recorded ramp baseline currents (see Methods for details) that changed polarity at positive potentials, consistently with a cation conductance (E_{rev} 22 ± 7mV, n = 11). Exposure to pulsed infrared light induced a fast increase in ramp currents that reaches its peak after 10 seconds (T_{peak} = 9.8 ± 2 s). An increase in current density was detected at both positive and negative potentials (Figure 3E, red columns) and reversed at voltages comparable with respect to controls (21 ± 10 mV). Astrocytes transfected with scrambled siRNA showed current responses similar in magnitude

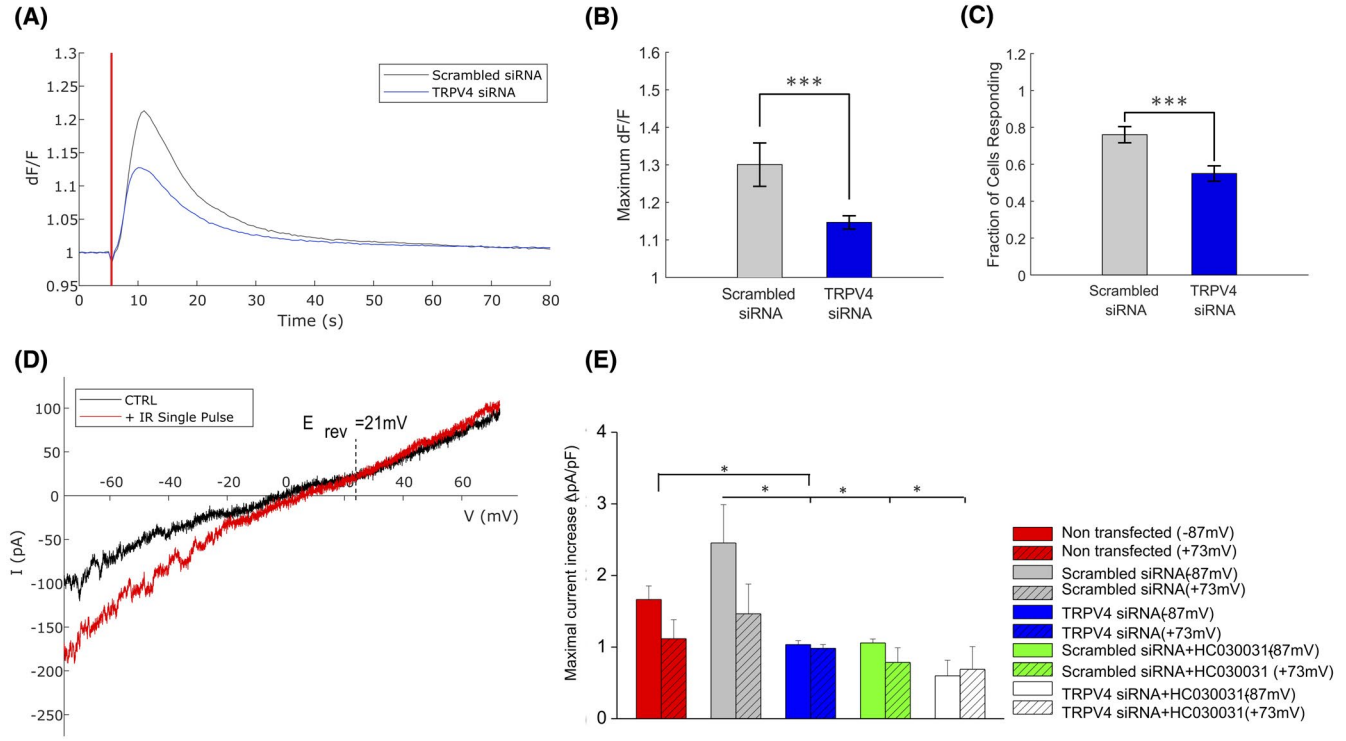

FIGURE 3 Study of the role of TRPV4 in the $[Ca^{2+}]_i$ increase and whole-cell conductance evoked by infrared stimulation in rat primary astrocytes. A, Representative traces of $[Ca^{2+}]_i$ dynamics recorded in astrocytes transfected with scrambled siRNA and TRPV4 siRNA. Red line represents the infrared stimulation time point. B and C, Bar plots showing the averaged maximal dF/F (B) and activation probability (C) in astrocytes transfected with scrambled siRNA (grey columns) and TRPV4 siRNA (blue columns). D, Typical ramp current traces stimulated with a voltage ramp protocol recorded in saline solution before (black trace) and at maximal current increase observed after pulsed infrared light (red trace). Dashed line depicts the reversal potential (E_{rev}) of the infrared stimulation-induced current. E, Bar plot of averaged maximal current density, recorded at −87 mV and + 73 mV after infrared stimulation, normalized with respect to the baseline current. Data were recorded in nontransfected primary rat astrocytes, (ΔpA/pF = 1.12 ± 0.26 at + 73mV; ΔpA/pF = 1.66 ± 0.19 at −87mV red columns, n = 11), in astrocytes transfected with scrambled siRNA, (ΔpA/pF = 1.46 ± 0.41 at + 73 mV, ΔpA/pF = 2.45 ± 0.54 at −87mV, grey columns, n = 6) or with TRPV4siRNA (ΔpA/pF = 0.98 ± 0.05 at + 73mV, ΔpA/pF = 1.03 ± 0.05 at −87mV, blue columns, n = 6, *P*val = .016 vs non transfected, *P*val = .0101 vs Scrambled siRNA). The plot also reported the averaged data in cells transfected with scrambled siRNA + 40 μM HC-030031 (ΔpA/pF = 1.06 ± 0.06 at −87 mV, ΔpA/pF = 0.79 ± 0.2 at + 73 mV green columns, n = 4, *P*val = .04), and TRPV4siRNA + 40μM HC-030031 (ΔpA/pF = 0.60 ± 0.21 at −87 mV, ΔpA/pF = 0.69 ± 0.31 at + 73 mV, white columns, n = 4, *P*val = .023). (Data are reported as mean and SEM. Student's *t* test, n = number of cells, Student's *t* test, **P* < .05; ***P* < .01). All experiment presented in this figure were performed using primary rat cortical astrocytes

(Figure 3E grey columns) and dynamics (T_{peak} = 9.7 ± 3 s) to those observed in nontransfected cells. Infrared-evoked current responses were negligible for both inward and outward currents in TRPV4 siRNA astrocytes (Figure 3E, blue columns). The onset of the infrared-evoked current was delayed in TRPV4 siRNA (T_{peak} = 34±3 s). Interestingly, the addition of HC-030031 (blocking TRPA1) decreased both inward and outward current density changes elicited by infrared stimulation in scrambled siRNA (Figure 3E, green columns) and nulled the residual responses in TRPV4 siRNA treated cells (Figure 3E, white columns). Collectively, these results suggest that TRPV4 and TRPA1 are both involved in mediating astrocytic extracellular Ca^{2+} influx and conductance increases in response to pulsed infrared light. The notion that TRPA1 is critical for regulation of basal $[Ca^{2+}]_i$ in astrocytes in vitro and in situ[36] may account for its involvement in the onset of the $[Ca^{2+}]_i$ responses and the relative decrease in dF/F magnitude when it is inhibited (Supporting Table S1, Figure 2E).

3.3 | Water transport is triggered by infrared stimulation

Given the partnership of TRP channels with AQP4 in astrocytes,[11] we hypothesized that the activation of TRPV4 and TRPA1 may be related to AQP4 and related astrocytic cell volume changes. To validate this hypothesis, astrocytes from wild-type (WT) mice and AQP4 knockout (KO) mice were modulated with pulsed infrared light and compared. Calcium imaging results show that AQP4 expression is critical to the magnitude and dynamics of the response of astrocytes to

infrared stimulation. When compared with WT, AQP4$^{(-/-)}$ astrocytes showed a decrease in both peak dF/F (Figure 4A,B) and activation probability (Figure S4C). Deletion of AQP4 caused a significantly delayed onset, with a nearly 50% increase in T_{peak} (Figure 4C) and a prolonged $T_{1/2}$ compared to WT astrocytes (Figure S4D). Accordingly, in differentiated astrocytes plated on nanostructured hydrotalcite (HTlc) films, where AQP4 expression and water permeability are increased,[33] the peak dF/F, and activation probability were increased with increased time to peak using infrared stimulation (Table S1, Figure 4, and Figure S4).

Remarkably, by performing a calcein fluorescence self-quenching assay,[34] we found that pulsed infrared light consistently induced water transport resulting in swelling and shrinkage of primary rat cortical astrocytes. Changes in cell volume appear in spatially distinct domains surrounding the site of stimulation. Nearly 50% of calcein-loaded astrocytes (505 responding, 526 nonresponding, n = 1031 cells) showed changes in levels of fluorescence immediately after the laser light was delivered (Figure 5A). About half of responding cells (n = 255) responded with decrease in fluorescence (shrinking), while the remaining responded with fluorescence increase (swelling). Interestingly, the magnitude of swelling as demonstrated by the increase in fluorescence (0.57 ± 0.38%) was different from that of shrinkage, that is, the decrease in fluorescence (−1.39 ± 1.01%). The time constant of cell swelling was faster (0.44 ± 0.04) than that observed for cell shrinkage (0.01 ± 0.02).

The spatial map of change in fluorescence following infrared stimulation as shown in Figure 5B, indicates that the cells directly under the fiber delivering infrared light shrunk in volume, while those located radially distal from the fiber illumination showed swelling. These results show that infrared stimulation induces both swelling and shrinkage in primary rat cortical astrocytes in spatially distinct domains surrounding the site of stimulation. These changes suggest that homeostatic osmotic responses may be triggered by this method.

3.4 | Proposed mechanisms

Various hypothesis can be proposed to explain the mechanisms underlying the effect of pulsed infrared light on astrocytes based on the experimental results described (Figure 6). Previous studies suggest that in electrically excitable and

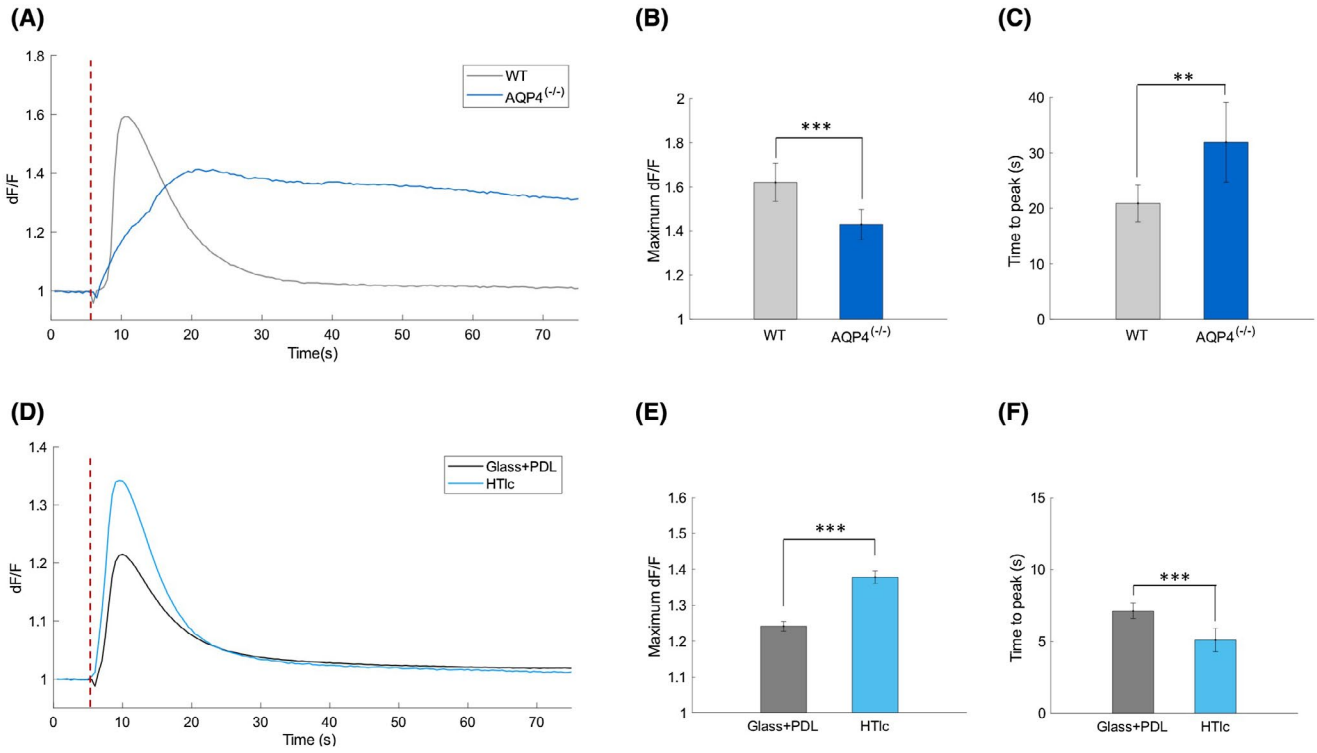

FIGURE 4 AQP4 expression is determinant for the dynamic of infrared-evoked calcium response. A, Representative traces of calcium fluorescence recorded in primary astrocytes from WT (light grey trace) and AQP4-KO ($^{-/-}$) mice (dark blue trace). B and C, Histogram plots showing averaged maximal dF/F (B) and time to peak (C) in astrocytes from WT (light grey columns) and AQP4-KO ($^{-/-}$) astrocytes (dark blue columns). D, Representative traces of calcium imaging experiments reporting dF/F dynamics performed on rat astrocytes grown on PDL (black trace) and on HTlc films (light blue trace). E and F, Histogram plots showing averaged maximal dF/F (E) and time to peak (F) in rat primary astrocytes grown on PDL (grey columns) and HTlc films (light blue columns). All histogram plots represent mean and error bars represent SEM. Student's *t* test, *$P < .05$; *$P < .01$; ***$P < .001$). Red dashed line in A and D represents the timepoint, where pulsed infrared light was delivered

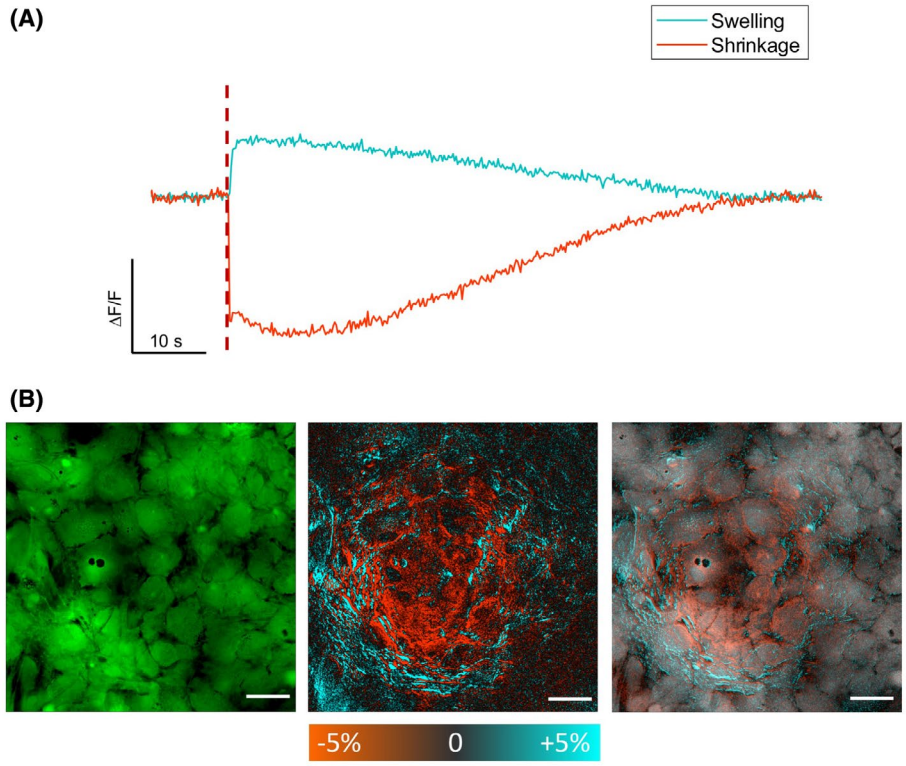

FIGURE 5 Water permeability is triggered by infrared pulses in rat astrocytes. A, Representative traces of calcein fluorescence recorded in rat astrocytes representing fluorescence somatic response to an infrared pulse. Red dashed line represents the time point at which the pulse INS was delivered. B, left panel: image of dF/F recorded one second before the laser pulse, center panel: spatial map of fluorescence changes following infrared laser pulse exposure, merge of the images is indicative of the spatial distribution of the response. Scale bars are 50 μM

non-excitable cell models, infrared stimulation initiates a mechano-electrical effect at the cell plasma membrane, transiently modulating its thickness, capacitance, and its lipid bilayer structure.[30,32] If direct gating of AQP4 by temperature rise is unlikely, the transient thermal gradient generated by infrared stimulation may spatially alter the kinetic energy of the water molecules around and within the cell,[47] driving water transport through the cells. It is also possible that the laser light modulates the lipid bilayer composition or fluidity in the extracellular membrane,[48] thus, initiating water transport and swelling/shrinkage through AQP4-independent pathways. As a result, AQP4 may accelerate or add to an already infrared-initiated event that increases swelling/shrinkage rate.

Previous studies report the activation of TRPV4 by infrared stimulation in spiral and vestibular ganglion neuron.[43,44] However, our data suggest that TRPV4 is not directly activated by pulsed infrared light in astrocytes, but rather as a secondary response to some additional effector. Function of TRPV4 is known to be dependent on osmotic stress,[5,11,13,49] basal $[Ca^{2+}]_i$,[5,36] that in the present case may be controlled in part by TRPA1 or IP_3R.

Given the known affinity and interaction between IP_3 and TRPV4,[49] it is possible that the activation of TRPV4 that we observed is dependent by the production of IP_3 induced by osmotic stress or by the increase in $[Ca^{2+}]_i$.[50] Accordingly, pulses of infrared light activated phospholipase-C mediated rises in $[Ca^{2+}]_i$ HT22 mouse hippocampal neurons and U87 human glioblastoma cells, suggesting the formation of IP_3.[40] However, our results do not provide evidence for IP_3 production by IR light in astrocytes, but only of activation of IP_3R by pulsed IR light.

Direct thermal activation of TRPA1 is unlikely, as its debated thermal activation is prominently for cold stimuli rather than warm.[7,36] A recent work suggested a direct activation of TRPA1 by transient heat induced by ultrafast infrared laser pulse,51 but the temperature-time dynamics explored were quite different from those explored in this study. Interestingly, a recent study reported the implication of TRPA1 in osmotic-induced Ca^{2+} influx.[52] While its activity and expression patterns is modulated by membrane lipid surrounding environment,[7] which might explain the role of TRPA1 during infrared stimulation. In summary, we hypothesize that infrared stimulation induces transmembrane water transport or alteration in lipid membrane composition, which in turn activates TRPA1. This activation initiates Ca^{2+} entry, promoting Ca^{2+} release via IP_3R, increased in $[Ca^{2+}]_i$ might bind to TRPV4 and sensitizes it to the cell volume changes triggered by pulsed infrared light (Figure 6).

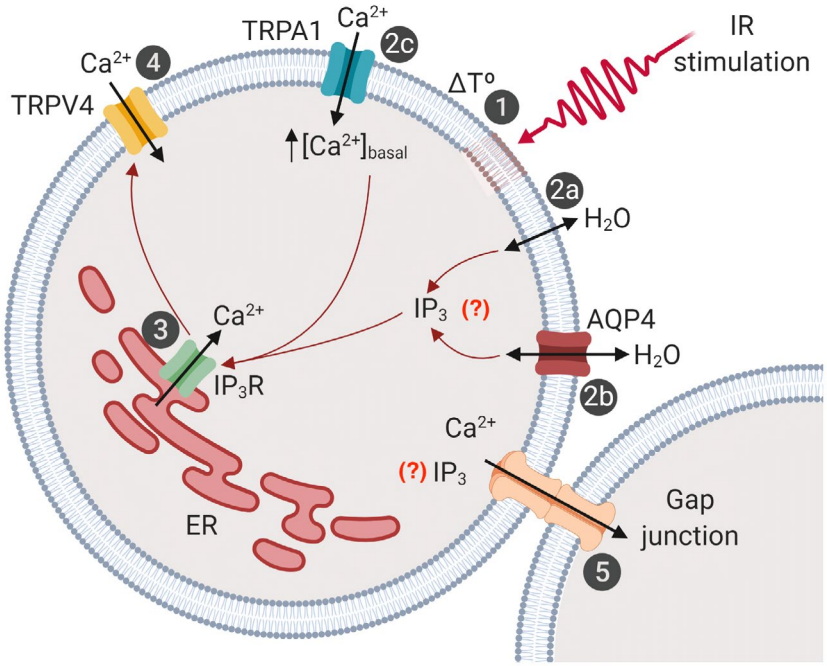

FIGURE 6 Possible mechanism underpinning the effects of infrared stimulation in astrocytes. Infrared pulse effects a thermal increase that can alter astroglial plasma membrane structure (thickness, fluidity, permeability) or osmotic gradient, (1). The alteration can allow water fluxes through the plasma membrane (2a) and through AQP4 (2b). Cell volume changes and/or mechanical membrane stress or incidental lipid release induced by infrared stimulation might activate TRPA1 (2a). Ca^{2+} influx through TRPA1 can elicit Ca^{2+} induced Ca^{2+} release via IP_3R (3). We hypothesize that $[Ca^{2+}]_i$ released via IP_3R path can bind TRPV4 and sensitize it to cell volume changes to initiate RVD or RVI (4). Lastly, the Ca^{2+} signal can travel through gap junctions to spread to neighboring cells (5). Given that osmotic stress via the arachidonic acid path to induce the production of IP_3,[49] we cannot rule out that the increase of IP_3 is involved in the effect (?) or on its propagation from cell to cell

4 | LIMITATIONS

In this study, our experiments only addressed a narrow range of possible physiological responses that infrared stimulation may be driving in astrocytes. As a cell that is integral to so many dynamic processes in the brain, we cannot conclusively state that water transport and intracellular calcium dynamics are the only driving responses triggered in astrocytes. Further, our study only sought to understand acute astrocytic responses to IR exposure. Chronic effects of IR exposure on astrocytes are actively being studied. Nonetheless, our work provides a basis for how pulsed infrared light affects acute astrocyte physiology.

Activation of cortical astrocytes in conjunction with neuronal cells when using infrared stimulation has been previously demonstrated in vivo.[29] However, questions remained on whether this response is a direct effect of this light on astrocytes or neurons with the other being affected indirectly. Here, we show that astrocytes respond to pulsed infrared light, suggesting that we must consider how astrocytes might be affecting neuronal activity during infrared stimulation of the brain. On the contrary, previous studies have shown that neurons also respond to infrared light. Thus, future studies using co-cultures and controlled multicellular preparations must be conducted to evaluate the selectivity (or lack thereof) of this approach in different cell types and their interplay.

The specificity of laser parameters needed to modulate specific cell types remains to be determined. Moreover, our study only probed short, 8 ms pulses of infrared light and delivered to a group of cells primarily targeting the cell body. However, pulsed infrared light has been demonstrated using a wide range of laser parameters.[53] The spatial and temporal scale of calcium dynamics in astrocytes appears to vary depending on the initiation of Ca^{2+} signals in the cell body, processes, or endfeet.[54,55] By modifying the illumination geometry of the fiber as well as varying laser parameters, spatially, and temporally, we may be able to trigger cellular or subcellular responses for tightly controlled multiscale probing and analyses of astrocytic $[Ca^{2+}]_i$ to study their function and dysfunction in various models.

5 | IMPLICATIONS

We have recently demonstrated that it is possible to evoke astrocytic Ca2+ responses mediated by TRPV4, TRPA1 as well as cell swelling with electrical stimulation[21] by organic cell stimulating and sensing device. Previous attempts from other groups to evoke astrocytic Ca^{2+} responses with light in cell

cultures were only successful when used with cell-conjugated NIR-optimized plasmonic nanostructures or label-free with high-intensity ultrafast NIR laser pulses.[56-58] Practically, our method of stimulation offers a label free, touchless strategy of glial and neural modulation - without exogenous effectors or genetic modification. A recent study indicates that commonly used visible light illumination protocols increase the temperature by 0.2-2°C and suppress spiking in multiple brain regions.[59] Now, this work raises questions on the assumption that astrocyte functions are not altered by thermal or optical modulation such as that used during two-photon imaging of calcium dynamics imaging in situ and in vivo. This calls for detailed investigation of the impact of light on neural cell function. Regardless, infrared stimulation may be a useful tool for studying astrocytic water and ionic dynamics and the effect of homeostasis, neuro-vascular coupling, and osmotic stress in healthy and pathological brain function.

6 | CONCLUSION

In conclusion, we have demonstrated for the first time that astrocytes can directly and dynamically respond to pulsed infrared light. We provide clear and consistent evidence of the molecular mechanisms initiating the response, as well as downstream effects that have a direct impact on physiologically relevant astrocyte function. Specifically, we have (a) characterized the initiation of Ca^{2+} responses in astrocytes from a label-free single 8 ms pulse of infrared light in terms of $[Ca^{2+}]_i$ dynamics, whole-cell cationic conductance, and water permeability, (b) identified specific molecular players that underpin the effect of infrared stimulation on astroglial cells, highlighting that activation of IP_3R path for $[Ca^{2+}]_i$, TRPA1, TRPV4, and AQP4 are all involved in shaping the dynamics of infrared-evoked $[Ca^{2+}]_i$ activity, (c) demonstrated that infrared stimulation is a valuable tool to study Ca^{2+} and water dynamics as well as regulatory volume responses in cultured astrocytes, which may be useful in studying these processes during homeostatic dysregulation or exploring the effects of astrocyte activity on neuronal signaling. Such tools can probe the ionic and osmotic dynamics of the brain on a cellular and whole-organ scale and modulate homeostatic function in astrocytes at high spatial and temporal precision that would enable the study of healthy and diseased brain function.

ACKNOWLEDGMENTS

This work was supported by EU Marie Curie Project OLIMPIA (GA 316832), the ASEE NDSEG Fellowship Program, and by the AFOSR Research Projects ASTROMAT, FA9550 16-1-0502, ASTRONIR, FA9550-17-1-0502 and FA9550-18-1-0255, 3D NEUROGLIA, DURIP FA9550-15-1-0328, FA9550-14-1-0303, FA 9550-17-1-0374. Calcium and calcein fluorescence imaging experiments were performed in part through the use of the Vanderbilt Cell Imaging Shared Resource (supported by NIH grants CA68485, DK20593, DK58404, DK59637, and EY08126). We are grateful to Dr Alessia Minardi from FABIT Department of the University of Bologna, for her help in the preparation and maintenance of astrocytes primary culture.

CONFLICT OF INTEREST

The authors decleare they have no conflict of interest.

AUTHOR CONTRIBUTIONS

A.I. Borrachero-Conejo and W.R. Adam prepared and maintained rat primary culture, performed, and analyzed the calcium imaging and experiment, performed the water transport experiments, contributed to the manuscript preparation and editing. E. Saracino prepared and maintained rat primary culture, performed patch-clamp experiments and analyzed the data. T. Posati performed the synthesis and fabrication of hydrotalcite (HTlc) films. M. Wang analyzed the calcium imaging data. M.G. Mola and G.P. Nicchia analyzed the calcein fluorescence data, prepared and maintained astrocytes primary culture from WT and AQP4 KO. M. Caprini and F. Formaggio provided animal facility for rat primary culture preparation, designed siRNA and performed siRNA transfection. M. De Bellis. and A. Frigeri provided AQP4, WT, and KO models, including breeding and genotyping of these animals. M. Muccini, R. Zamboni, M.R. Hutchinson contributed to the discussion of the results and editing of the manuscript. A. Mahadevan-Jansen and V. Benfenati are the overall principal investigators of the project. They coordinated the research effort, designed the experiments, defined the mechanism of infrared stimulation in astrocyte, wrote, and finalized the manuscript.

REFERENCES

1. Verkhratsky A, Nedergaard M. Physiology of astroglia. *Physiol Rev*. 2018;98:239-389.
2. Santello M, Toni N, Volterra A. Astrocyte function from information processing to cognition and cognitive impairment. *Nat Neurosci*. 2019;22:154-166.
3. Formaggio F, Saracino E, Mola MG, et al. LRRC8A is essential for swelling-activated chloride current and for regulatory volume decrease in astrocytes. *FASEB J*. 2019;33:101-113.
4. Benfenati V, Ferroni S. Water transport between CNS compartments: functional and molecular interactions between aquaporins and ion channels. *Neuroscience*. 2010;168:926-940.
5. Benfenati V, Amiry-Moghaddam M, Caprini M, et al. Expression and functional characterization of transient receptor potential vanilloid-related channel 4 (TRPV4) in rat cortical astrocytes. *Neuroscience*. 2007;148:876-892.
6. Butenko O, Dzamba D, Benesova J, et al. The increased activity of TRPV4 channel in the astrocytes of the adult rat hippocampus after cerebral hypoxia/ischemia. *PLoS ONE*. 2012;7:e39959.
7. Startek JB, Boonen B, López-Requena A, et al. Mouse TRPA1 function and membrane localization are modulated by direct interactions with cholesterol. *eLife*. 2019;8:e46084.

8. Garcia-Elias A, Mrkonjic S, Pardo-Pastor C, et al. Phosphatidylinositol-4,5-biphosphate-dependent rearrangement of TRPV4 cytosolic tails enables channel activation by physiological stimuli. *Proc Natl Acad Sci U S A*. 2013;110:9553-9558.
9. Nilius B, Vriens J, Prenen J, Droogmans G, Voets T. TRPV4 calcium entry channel: a paradigm for gating diversity. *Am J Physiol Cell Physiol*. 2004;286:C195-C205.
10. Startek JB, Boonen B, Talavera K, Meseguer V. TRP channels as sensors of chemically-induced changes in cell membrane mechanical properties. *Int J Mol Sci*. 2019;20:371.
11. Benfenati V, Caprini M, Dovizio M, et al. An aquaporin-4/transient receptor potential vanilloid 4 (AQP4/TRPV4) complex is essential for cell-volume control in astrocytes. *Proc Natl Acad Sci U S A*. 2011;108:2563-2568.
12. Thrane AS, Rappold PM, Fujita T, et al. Critical role of aquaporin-4 (AQP4) in astrocytic Ca2+ signaling events elicited by cerebral edema. *Proc Natl Acad Sci U S A*. 2011;108:846-851.
13. Jo AO, Ryskamp DA, Phuong TTT, et al. TRPV4 and AQP4 channels synergistically regulate cell volume and calcium homeostasis in retinal müller glia. *J Neurosci*. 2015;35:13525-13537.
14. Mola MG, Sparaneo A, Gargano CD, et al. The speed of swelling kinetics modulates cell volume regulation and calcium signaling in astrocytes: a different point of view on the role of aquaporins. *Glia*. 2016;64:139-154.
15. Nicchia GP, Pisani F, Simone L, et al. Glio-vascular modifications caused by aquaporin-4 deletion in the mouse retina. *Exp Eye Res*. 2016;146:259-268.
16. Noell S, Wolburg-Buchholz K, Mack AF, et al. Dynamics of expression patterns of AQP4, dystroglycan, agrin and matrix metalloproteinases in human glioblastoma. *Cell Tissue Res*. 2012;347:429-441.
17. Nicchia GP, Nico B, Camassa LMA, et al. The role of aquaporin-4 in the blood-brain barrier development and integrity: studies in animal and cell culture models. *Neuroscience*. 2004;129:935-945.
18. Yool AJ, Brown EA, Flynn GA. Roles for novel pharmacological blockers of aquaporins in the treatment of brain oedema and cancer. *Clin Exp Pharmacol Physiol*. 2010;37:403-409.
19. Mederos S, Hernández-Vivanco A, Ramírez-Franco J, et al. Melanopsin for precise optogenetic activation of astrocyte-neuron networks. *Glia*. 2019;67:915-934.
20. Benfenati V, Martino N, Antognazza MR, et al. Photostimulation of whole-cell conductance in primary rat neocortical astrocytes mediated by organic semiconducting thin films. *Adv Healthc Mater*. 2014;3:392-399.
21. Borrachero-Conejo AI, Saracino E, Natali M, et al. Electrical stimulation by an organic transistor architecture induces calcium signaling in nonexcitable brain cells. *Adv Healthc Mater*. 2019;8:e1801139.
22. Benfenati V, Toffanin S, Bonetti S, et al. A transparent organic transistor structure for bidirectional stimulation and recording of primary neurons. *Nature Materials* 2013;12:672-680.
23. Maya-Vetencourt JF, Ghezzi D, Antognazza MR, et al. A fully organic retinal prosthesis restores vision in a rat model of degenerative blindness. *Nature Materials*. 2017;16:681-689.
24. Cho W-H, Barcelon E, Lee SJ. Optogenetic glia manipulation: possibilities and future prospects. *Exp Neurobiol*. 2016;25:197-204.
25. Wells J, Kao C, Konrad P, et al. Biophysical mechanisms of transient optical stimulation of peripheral nerve. *Biophys J*. 2007;93:2567-2580.
26. Wells J, Kao C, Mariappan K, et al. Optical stimulation of neural tissue in vivo. *Opt Lett*. 2005;30:504-506.
27. Cayce JM, Kao CC, Malphrus JD, Konrad PE, Mahadevan-Jansen A, Jansen ED. Infrared neural stimulation of thalamocortical brain slices. *IEEE J Select Topics Quantum Electron*. 2010;16:565-572.
28. Cayce JM, Wells JD, Malphrus JD, et al. Infrared neural stimulation of human spinal nerve roots in vivo. *Neurophotonics*. 2015;2:015007.
29. Cayce JM, Bouchard MB, Chernov MM, et al. Calcium imaging of infrared-stimulated activity in rodent brain. *Cell Calcium*. 2014;55:183-190.
30. Shapiro MG, Homma K, Villarreal S, Richter C-P, Bezanilla F. Infrared light excites cells by changing their electrical capacitance. *Nat Commun*. 2012;3:736.
31. Ebtehaj Z, Hatef A, Malekmohammad M, Soltanolkotabi M. Computational modeling and validation of thermally induced electrical capacitance changes for lipid bilayer membranes irradiated by pulsed lasers. *J Phys Chem B*. 2018;122:7319-7331.
32. Plaksin M, Shapira E, Kimmel E, Shoham S. Thermal transients excite neurons through universal intramembrane mechanoelectrical effects. *Phys Rev X*. 2018;8:011043.
33. Posati T, Pistone A, Saracino E, et al. A nanoscale interface promoting molecular and functional differentiation of neural cells. *Sci Rep*. 2016;6:31226.
34. Solenov E, Watanabe H, Manley GT, Verkman AS. Sevenfold-reduced osmotic water permeability in primary astrocyte cultures from AQP-4-deficient mice, measured by a fluorescence quenching method. *Am J Physiol Cell Physiol*. 2004;286:C426-C432.
35. Schindelin J, Arganda-Carreras I, Frise E, et al. Fiji: an open-source platform for biological-image analysis. *Nat Methods*. 2012;9:676-682.
36. Shigetomi E, Jackson-Weaver O, Huckstepp RT, O'Dell TJ, Khakh BS. TRPA1 channels are regulators of astrocyte basal calcium levels and long-term potentiation via constitutive D-serine release. *J Neurosci*. 2013;33:10143-10153.
37. Hofer AM, Fasolato C, Pozzan T. Capacitative Ca2+ entry is closely linked to the filling state of internal Ca2+ stores: a study using simultaneous measurements of ICRAC and intraluminal [Ca2+]. *J Cell Biol*. 1998;140:325-334.
38. Benfenati V, Caprini M, Nicchia GP, et al. Carbenoxolone inhibits volume-regulated anion conductance in cultured rat cortical astroglia. *Channels*. 2009;3:323-336.
39. Scemes E. Components of astrocytic intercellular calcium signaling. *Mol Neurobiol*. 2000;22:167-179.
40. Moreau D, Lefort C, Pas J, Bardet SM, Leveque P, O'Connor RP. Infrared neural stimulation induces intracellular Ca2+ release mediated by phospholipase C. *J Biophotonics*. 2018;11.
41. Tolstykh GP, Olsovsky CA, Ibey BL, Beier HT. Ryanodine and IP3 receptor-mediated calcium signaling play a pivotal role in neurological infrared laser modulation. *Neurophotonics*. 2017;4:025001.
42. Sherwood MW, Arizono M, Hisatsune C, et al. Astrocytic IP3 Rs: Contribution to Ca2+ signalling and hippocampal LTP. *Glia*. 2017;65:502-513.
43. Barrett JN, Rincon S, Singh J, et al. Pulsed infrared releases Ca2+ from the endoplasmic reticulum of cultured spiral ganglion neurons. *J Neurophysiol*. 2018;120:509-524.
44. Lumbreras V, Bas E, Gupta C, Rajguru SM. Pulsed infrared radiation excites cultured neonatal spiral and vestibular ganglion neurons by modulating mitochondrial calcium cycling. *J Neurophysiol*. 2014;112:1246-1255.

45. Paris L, Marc I, Charlot B, Dumas M, Valmier J, Bardin F. Millisecond infrared laser pulses depolarize and elicit action potentials on in-vitro dorsal root ganglion neurons. *Biomed Opt Express*. 2017;8:4568-4578.
46. Vincent F, Acevedo A, Nguyen MT, et al. Identification and characterization of novel TRPV4 modulators. *Biochem Biophys Res. Commun*. 2009;389:490-494.
47. Nicchia GP, Frigeri A, Liuzzi GM, et al. Aquaporin-4-containing astrocytes sustain a temperature- and mercury-insensitive swelling in vitro. *Glia*. 2000;31:29-38.
48. Walsh AJ, Cantu JC, Ibey BL, Beier HT. Short infrared laser pulses increase cell membrane fluidity. Presented at: SPIE BiOS; 2017; San Francisco, CA.
49. Fernandes J, Lorenzo IM, Andrade YN, et al. IP3 sensitizes TRPV4 channel to the mechano- and osmotransducing messenger 5'-6'-epoxyeicosatrienoic acid. *J Cell Biol*. 2008;181:143-155.
50. Garcia-Elias A, Lorenzo IM, Vicente R, Valverde MA. IP3 receptor binds to and sensitizes TRPV4 channel to osmotic stimuli via a calmodulin-binding site. *J Biol Chem*. 2008;283:31284-31288.
51. Ermakova YG, Lanin AA, Fedotov IV, et al. Thermogenetic neurostimulation with single-cell resolution. *Nat Commun*. 2017;8:15362.
52. Fujita F, Uchida K, Takayama Y, Suzuki Y, Takaishi M, Tominaga M. Hypotonicity-induced cell swelling activates TRPA1. *J Physiol Sci*. 2018;68:431-440.
53. Thompson AC, Stoddart PR, Jansen ED. Optical stimulation of neurons. *Curr Mol Imaging*. 2014;3:162-177.
54. Dunn KM, Hill-Eubanks DC, Liedtke WB, Nelson MT. TRPV4 channels stimulate Ca2+-induced Ca2+ release in astrocytic endfeet and amplify neurovascular coupling responses. *Proc Natl Acad Sci U S A*. 2013;110:6157-6162.
55. Bindocci E, Savtchouk I, Liaudet N, Becker D, Carriero G, Volterra A. Three-dimensional Ca2+ imaging advances understanding of astrocyte biology. *Science*. 2017;356.
56. Choi M, Yoon J, Ku T, Choi K, Choi C. Label-free optical activation of astrocyte in vivo. *J Biomed Opt*. 2011;16:075003.
57. Eom K, Hwang S, Yun S, Byun KM, Jun SB, Kim SJ. Photothermal activation of astrocyte cells using localized surface plasmon resonance of gold nanorods. *J Biophotonics*. 2017;10:486-493.
58. Zhao Y, Zhang Y, Liu X, et al. Photostimulation of astrocytes with femtosecond laser pulses. *Opt Express*. 2009;17:1291-1298.
59. Owen SF, Liu MH, Kreitzer AC. Thermal constraints on in vivo optogenetic manipulations. *Nat Neurosci*. 2019;22:1061-1065.

SUPPORTING INFORMATION

Additional Supporting Information may be found online in the Supporting Information section.

How to cite this article: Borrachero-Conejo AI, Adams WR, Saracino E, et al. Stimulation of water and calcium dynamics in astrocytes with pulsed infrared light. *The FASEB Journal*. 2020;00:1–15. https://doi.org/10.1096/fj.201903049R